remote sensing

MDPI

Article

Earlier Spring-Summer Phenology and Higher Photosynthetic Peak Altered the Seasonal Patterns of Vegetation Productivity in Alpine Ecosystems

Fan Yang [1], Chao Liu [1], Qianqian Chen [1], Jianbin Lai [2] and Tiegang Liu [1,*]

[1] State Key Laboratory of Hydraulics and Mountain River Engineering, College of Water Resource and Hydropower, Sichuan University, Chengdu 610065, China; yangfan09@stu.scu.edu.cn (F.Y.); liuchao@scu.edu.cn (C.L.); chenqianqian@stu.scu.edu.cn (Q.C.)

[2] Key Laboratory of Ecosystem Network Observation and Modeling, Institute of Geographic Sciences and Natural Resources Research, Chinese Academy of Sciences, Beijing 100101, China; laijianbin@igsnrr.ac.cn

* Correspondence: liutiegang79@scu.edu.cn

Abstract: Carbon uptake of vegetation is controlled by phenology and photosynthetic carbon uptake capacity. However, our knowledge of the seasonal responses of vegetation productivity to phenological and physiological changes in alpine ecosystems is still weak. In this study, we quantified the spatio-temporal variations of vegetation phenology and gross primary productivity (GPP) across the source region of the Yellow River (SRYR) by analyzing MODIS-derived vegetation phenology and GPP from 2001 to 2019, and explored how vegetation phenology and maximum carbon uptake capacity (GPP_{max}) affected seasonal GPP over the region. Our results showed that the SRYR experienced significantly advanced trends ($p < 0.05$) for both start (SOS) and peak (POS) of the growing season from 2001 to 2019. Spring GPP (GPP_{spr}) had a significantly increasing trend ($p < 0.01$), and the earlier SOS had obvious positive effects on GPP_{spr}. Summer GPP (GPP_{sum}) was significantly and negatively correlated to POS ($p < 0.05$). In addition, GPP_{max} had a significant and positive correlation with GPP_{sum} and GPP_{ann} ($p < 0.01$), respectively. It was found that an earlier spring-summer phenology and higher photosynthetic peak enhanced the photosynthetic efficiency of vegetation in spring and summer and altered the seasonal patterns of vegetation productivity in the SRYR under warming and wetting climates. This study indicated that not only spring and autumn phenology but also summer phenology and maximum carbon uptake capacity should be regarded as crucial indicators regulating the carbon uptake process in alpine ecosystems. This research provides important information about how changes in phenology affect vegetation productivity in alpine ecosystems under global climate warming.

Keywords: alpine ecosystems; phenology; photosynthetic peak; gross primary productivity

Citation: Yang, F.; Liu, C.; Chen, Q.; Lai, J.; Liu, T. Earlier Spring-Summer Phenology and Higher Photosynthetic Peak Altered the Seasonal Patterns of Vegetation Productivity in Alpine Ecosystems. *Remote Sens.* **2024**, *16*, 1580. https://doi.org/10.3390/rs16091580

Academic Editors: Pamela L. Nagler and Shin Nagai

Received: 12 March 2024
Revised: 18 April 2024
Accepted: 27 April 2024
Published: 29 April 2024

1. Introduction

Gross primary productivity (GPP) is a key component of carbon cycling in terrestrial ecosystems [1,2]. As carbon sequestration in terrestrial ecosystems exhibits wide variability [3,4], quantifying the GPP variability in terrestrial ecosystems is imperative [5]. The carbon uptake of vegetation is controlled by phenology and photosynthetic carbon uptake capacity [3,4]. Vegetation phenology refers to the periodic timing of recurring biological events caused by the periodic changes of environmental factors such as precipitation and air temperature [6,7]. Vegetation phenology is sensitive to climate changes, and shifts of vegetation phenology affect the seasonal dynamics of GPP [3,8,9]. Maximum daily GPP (GPP_{max}) is an important physiological indicator which represents the maximum photosynthetic capacity of vegetation in the growing season [4,10]. Quantifying the impacts of phenological and physiological changes on seasonal vegetation productivity for various climatic zone and ecosystem types is essential to accurate assessments of the spatial and temporal variations in annual GPP at regional and global scales [11–13].

Shifts of vegetation phenology due to climate changes can affect vegetation productivity by affecting the process of carbon uptake [14–17]. Most of previous studies on vegetation phenology have demonstrated that the start of the growing season (SOS) and the end of the growing season (EOS) have, respectively, advanced and delayed trends under global warming [18–20]. Cheng et al. [21] found that earlier SOS and later EOS led to an extension of the length of growing season (LOS) in the Tibetan Plateau, resulting in an increase of the gross primary productivity of vegetation. The spatio-temporal responses of vegetation productivity to phenology may differ among various climatic zones and ecosystem types [22]. Chen et al. [23] reported that the increase of vegetation gross primary productivity in the eastern Tibetan Plateau was mainly due to the advance of the SOS rather than the delay of the EOS, whereas Zhang et al. [10] found that the delay of the EOS remarkably enhanced the GPP over the period from September to October for broadleaf forests in east China. In addition, a delayed EOS may not lead to a substantial increase of GPP due to weak photosynthetic efficiency and the limited ability of organic matter accumulation in autumn [24,25]. Most studies have focused on the effects of phenological factors (SOS, EOS and LOS) on vegetation productivity at the annual scale [13]. However, it is still unclear how phenology affects vegetation productivity at the seasonal scale, especially for the peak of growing season. Peak of growing season (POS) represents the timing of the seasonal peak canopy structure, which reflects the ability of terrestrial ecosystem productivity [26] and is an important phenology indicator for the carbon cycle of terrestrial ecosystems [27]. Besides vegetation phenology, GPP_{max} plays a crucial role in controlling the interannual variability of annual GPP [28,29]. GPP_{max} occurs in summer in northern temperate ecosystems [4] and is positively correlated with summer GPP [30]. Some studies have indicated that GPP_{max} even has a greater impact on variations of GPP_{ann} than phenology [4,10].

In recent years, the responses of vegetation productivity to shifting phenology in alpine ecosystems across Qinghai-Tibet Plateau (QTP) has been investigated, which mainly focused on the effects of the SOS, EOS and LOS on ecosystem productivity [22,31]. The alpine ecosystems on the QTP are highly sensitive to climate changes [13]. Zhu et al. [31] found that the warming climate in the Tibetan Plateau resulted in a later SOS for alpine meadow in spring due to water limitations but promoted ecosystem carbon uptake in summer with better moisture conditions. Wang et al. [22] found that most of the QTP experienced significant trends in advancing the SOS, delaying the EOS and prolonging the LOS in 2000 and 2012, and vegetation productivity also increased in most parts of the plateau. These studies mainly focused on the changes to SOS, EOS and LOS and their effects on annual productivity in the QTP, but few studies were concerned with the effects of vegetation phenology and photosynthetic capability on the seasonal dynamics of productivity in the region. Moreover, the response relationships between vegetation productivity and phenology were complex and varied within different climatic regimes due to differences of terrain and climate conditions in the QTP [22], and it is necessary to explore the response mechanisms of seasonal vegetation productivity to the phenology dynamics for various climatic zones.

The source region of the Yellow River (SRYR) is located in the northeast of the QTP, which is characterized by an alpine climate, and vegetation mainly consists of alpine steppe and alpine meadow [32] with obvious seasonality. Since 2000, both annual temperature and precipitation have seen increasing trends in the SRYR [33]. Moreover, the temperature has had a higher rate increase for the SRYR than that for the whole Tibetan Plateau [34,35], resulting in changes of the boundaries between seasonally frozen ground and permafrost [36]. An advanced trend of spring phenology in alpine meadow in the SRYR has been reported [37]. This paper aims to study the seasonal responses of vegetation productivity to phenology and physiology changes in alpine ecosystems. There are two objectives for this study: (1) examining the variations of vegetation phenology (SOS, POS, EOS and LOS), photosynthetic carbon uptake capacity (GPP_{max}) and GPP at seasonal and annual scales for the alpine ecosystems in the SRYR from 2001 to 2019 and (2) exploring the seasonal responses of annual GPP to the changes of vegetation phenology and photosynthetic capability. This study can help in understanding the effects of vegetation phenology on the carbon cycle in alpine ecosystems.

2. Materials and Methods

2.1. Study Area

The Yellow River is the second longest river in China, with length of 5464 km and basin area of 79.5 × 10^4 km^2. The source region of the Yellow River (Figure 1a) is located in the northeast of the Tibetan plateau (32.14~36.08°N, 95.77~102.97°E) and covers an area of 11.8 × 10^4 km^2, accounting for about 15% of the total area of the Yellow River Basin. The SRYR has complex landforms, including mountains, basins, canyons, lakes, alluvial plains and flood plains [32]. The altitude increases gradually from east to west, with an average elevation of 4500 m. The SRYR has a Qinghai-Tibet alpine climate, and the hydro-thermal conditions display a distinct northwest-southeast gradient [38]. The average annual precipitation increases from northwest to southeast, with an average of 545 mm, concentrated in the period from May to October, accounting for about 70% of the annual total precipitation [39]. The average annual temperature varies between −1.2 °C and 5.8 °C from the northwest to the southeast. The region is dominated by alpine meadow and alpine steppe (Figure 1c), which are very sensitive to climatic changes [40].

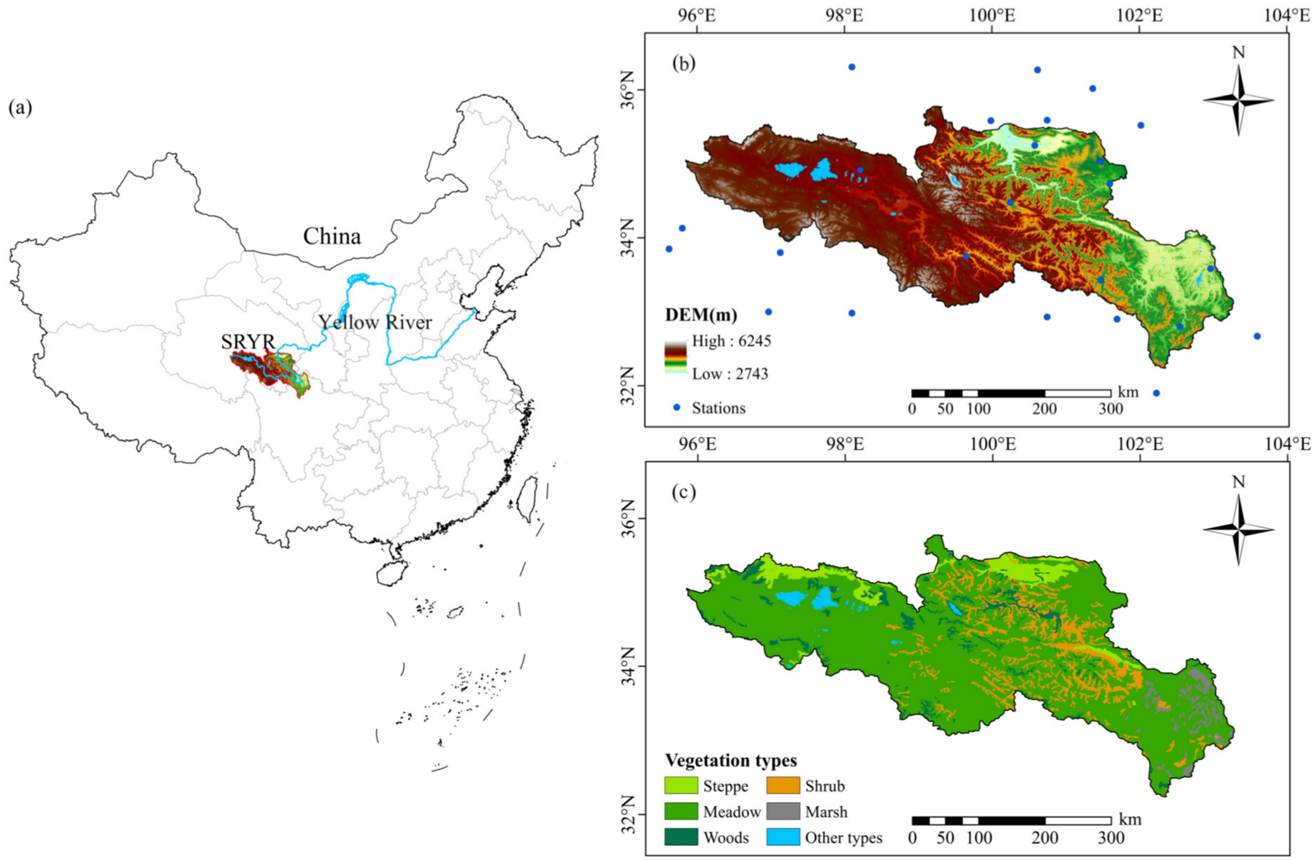

Figure 1. Location of the source region of the Yellow River (SRYR) (**a**); distribution of meteorological stations (**b**); vegetation types in the SRYR (**c**).

2.2. Data Source

2.2.1. Phenological Metrics

The MCD12Q2 (Collection 6) vegetation phenological dataset with a spatial resolution of 500 m and a time resolution of one year was derived from the Google Earth Engine platform from 2000 to 2019. This dataset is derived from thresholding the amplitudes of the time series of the 2-band enhanced vegetation index (EVI2) [41], which is computed from VIIRS Nadir BRDF (Bidirectional Reflectance Distribution Function)-Adjusted Reflectance (NBAR) product (8 days, 500 m) [42]. We extracted the greenup, peak and dormancy layer from the MCD12Q2 dataset as SOS, POS and EOS, respectively, and the LOS was defined as the length between the SOS and EOS [43]. SOS and EOS are defined as the date when the EVI first crossed 15% and last crossed 15% of the segment EVI amplitude, respectively, and POS is the date when the EVI reached the maximum of the segment EVI amplitude [43,44]. The MCD12Q2 dataset has been used in the studies of vegetation phenology changes in the QPT [45,46].

2.2.2. Meteorological Data

The meteorological data were derived from the National Meteorological Data Center (http://data.cma.cn, accessed on 4 January 2021). The monthly meteorological data, including precipitation and average air temperature from 24 stations in and around the SRYR from 2001 to 2019, were selected (Figure 1b, Table 1). The simple Kriging method was used to interpolate the meteorological data to raster data with a spatial resolution of 500 m.

Table 1. Longitude, latitude and elevation information of meteorological stations.

Station	Lon (°)	Lat (°)	Elevation (m)
Aba	101.70	32.90	3275.1
Zeku	101.47	35.03	3662.8
Hongyuan	102.55	32.80	3491.6
Ruoergai	102.97	33.58	3441.4
Maduo	98.22	34.92	4272.3
Dari	99.65	33.75	3967.5
Xinghai	99.98	35.58	3323.2
Henan	101.60	34.73	3500.0
Tongde	100.58	35.25	3148.2
Maerkang	102.23	31.90	2664.4
Shiqu	98.10	32.98	4200.0
Tongren	102.02	35.52	2491.4
Jiuzhi	101.48	33.43	3628.5
Qingshuihe	97.13	33.80	4415.4
Banma	100.75	32.93	3530.0
Dulan	98.10	36.31	3189.0
Qumalai	95.80	34.13	4175.0
Maqin	100.25	34.48	3719.0
Guinan	100.75	35.59	3120.0
Gonghe	100.62	36.27	2835.0
Guide	101.37	36.02	2237.1
Zhiduo	95.62	33.85	4179.1
Yushu	96.97	33.00	3716.9
Songpan	103.60	32.67	2850.7

2.2.3. Gross Primary Productivity Dataset

We selected the MODIS dataset of GPP products (MOD17A2H006) from the National Aeronautics and Space Administration (NASA) Earth Observation System Data and Information System (https://www.earthdata.nasa.gov, accessed on 10 June 2021). The data period is from 2001 to 2019, with a spatial resolution of 500 m and a temporal resolution of 8 d. The MODIS GPP dataset was developed based on the Light Use Efficiency model, and its reliability has been validated in various studies [47–49] and has been used in studies in the QPT [45]. Seasonal GPP for spring (March to May), summer (June to August), autumn (September to November) and winter (December to February) were synthesized based on 8-day GPP data, respectively. The maximum daily GPP in each year was extracted by the Maximum Value Composite method as GPP_{max}.

2.2.4. Other Datasets

The digital elevation model (DEM) data were from the Resource and Environmental Science Data Platform (http://www.resdc.cn, accessed on 21 June 2021), with a resolution of 30 m. According to the 1:1,000,000 digitized vegetation map of China [50] from the Environmental and Ecological Science Data Center for West China, the vegetation types in the SRYR can be divided into alpine meadow, alpine steppe, woods, shrub, marsh and other types, which account for 75.25%, 5.92%, 4.77%, 10.52%, 2.24% and 1.30%, respectively (Figure 1c).

2.3. Methods

2.3.1. Maximum Value Composite

Maximum Value Composite (MVC) was used to obtain the maximum daily GPP value [51] through an 8-day GPP data time series using ArcGIS 10.6 software (Environmental Systems Research Institute, 2018) [52]. The expression is as follows:

$$\mathrm{GPP}_{\mathrm{i,max}} = \mathrm{Max}(\mathrm{GPP}_{\mathrm{i,j}}) \tag{1}$$

where $\mathrm{GPP}_{\mathrm{i,max}}$ means the maximum daily GPP value in year i, and $\mathrm{GPP}_{\mathrm{i,j}}$ is the average daily value from the cumulative 8-day GPP composite value for the period j in year i.

2.3.2. Trend Analysis

In order to detect the temporal trends of climatic variables, vegetation phenology and seasonal and annual GPP in the SRYR over 19 years and their corresponding significance, the non-parametric Sen's slope method [53] and Mann–Kendall trend test [54,55] were applied. We used Matlab R2018b software (MathWorks, 2018) to analyze the data at the raster scale [56]. The slope β was calculated by the following equation:

$$\beta = Median\left(\frac{x_j - x_i}{j - i}\right), \forall j > i \tag{2}$$

where *Median* is a function of taking the median value, x_i and x_j are time series data; in this study, $2001 \leq i < j \leq 2019$.

2.3.3. Pearson Correlation Analysis

Pearson correlation analysis was used to examine the correlation between climate variables, vegetation phenology and seasonal and annual productivity, and the correlation coefficient r was calculated by the following equation:

$$r = \frac{\sum_{i=1}^{n}\left(X_i - \overline{X}\right)\left(Y_i - \overline{Y}\right)}{\sqrt{\sum\limits_{i=1}^{n}\left(X_i - \overline{X}\right)^2}\sqrt{\sum\limits_{i=1}^{n}\left(Y_i - \overline{Y}\right)^2}} \tag{3}$$

where r is the correlation coefficient of two variables, $\overline{X}$ and $\overline{Y}$ are the average values of the two variables in the time series, and n is the number of years. In addition, a t-test was used to test the significance of the correlations [57]. The correlation coefficients are significant at the 0.05 level with p values < 0.05, and are significant at the 0.01 level with p values < 0.01.

3. Results

3.1. Spatio-Temporal Variations of Precipitation and Air Temperature

Climate change showed a warming and wetting trend in the SRYR at annual and seasonal scales from 2001 to 2019. The average annual precipitation and air temperature were 545.2 ± 64.7 mm and 1.15 ± 0.39 °C, respectively. Both annual precipitation (Figure 2a) and air temperature (Figure 2b) had significantly increasing trends ($p < 0.05$) at rates of 6.37 mm yr^{-1} and 0.043 °C yr^{-1}, respectively. The average precipitation and air temperature in spring were, respectively, 107.1 ± 19.7 mm and 1.55 ± 0.56 °C, with significantly increasing trends at rates of 2.4 mm yr^{-1} ($p < 0.01$) (Figure 2c) and 0.034 °C yr^{-1} ($p < 0.05$) (Figure 2d), respectively. The average precipitation and air temperature in autumn were 125.2 ± 24.9 mm and 1.24 ± 0.66 °C, respectively. The autumn temperature also showed a significantly increasing trend ($p < 0.05$), with a rate of 0.065 °C yr^{-1} (Figure 2h), while autumn precipitation showed an insignificantly increasing trend ($p > 0.05$), with a rate of 1.54 mm yr^{-1} (Figure 2g). The average precipitation and temperature in summer were 297.6 ± 46.1 mm and 10.84 ± 0.62 °C, respectively. There were insignificant and increasing trends for both summer precipitation (+2.6 mm yr^{-1}, $p > 0.05$) (Figure 2e) and temperature (+0.041 °C yr^{-1}, $p > 0.05$) (Figure 2f).

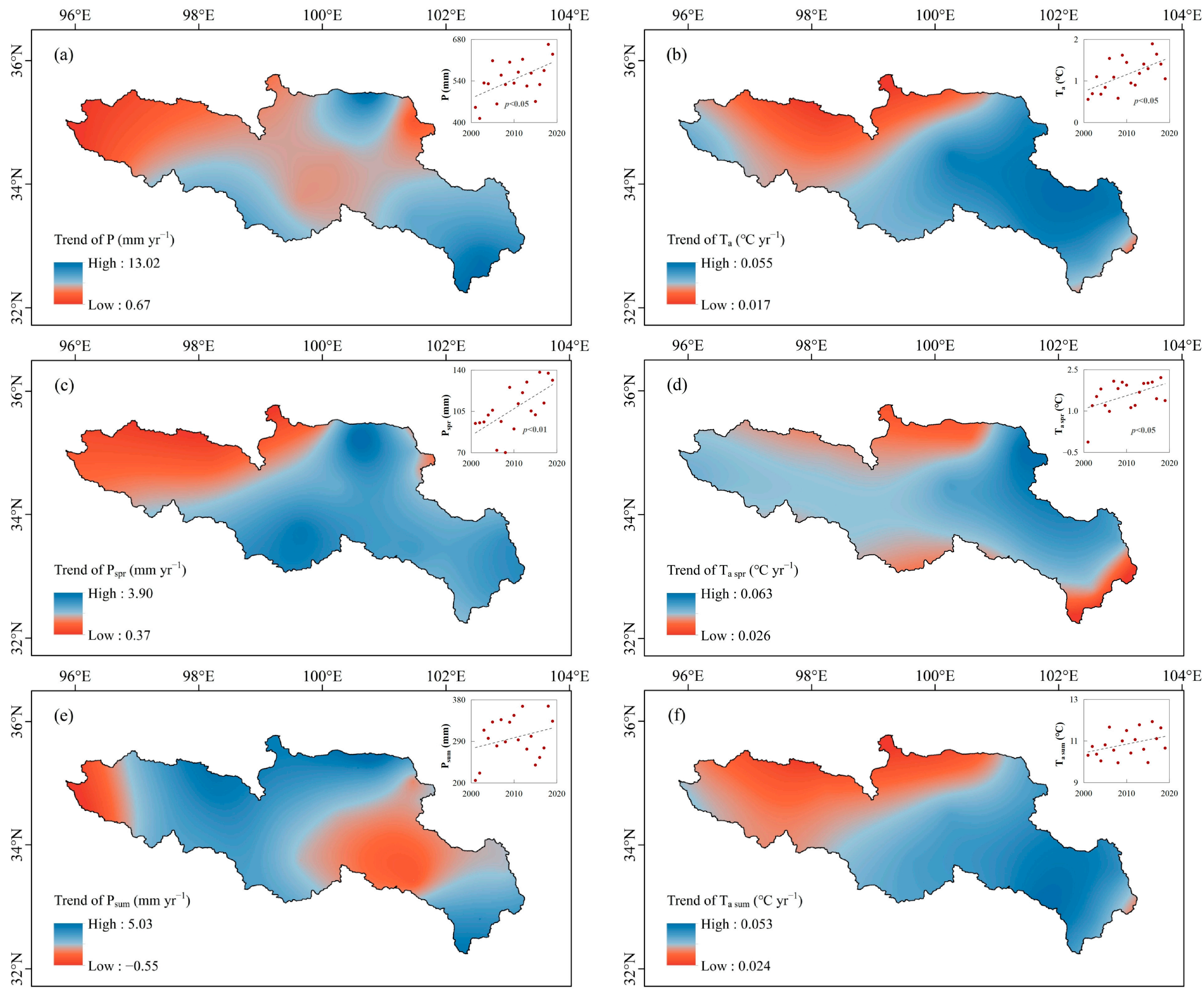

Figure 2. *Cont.*

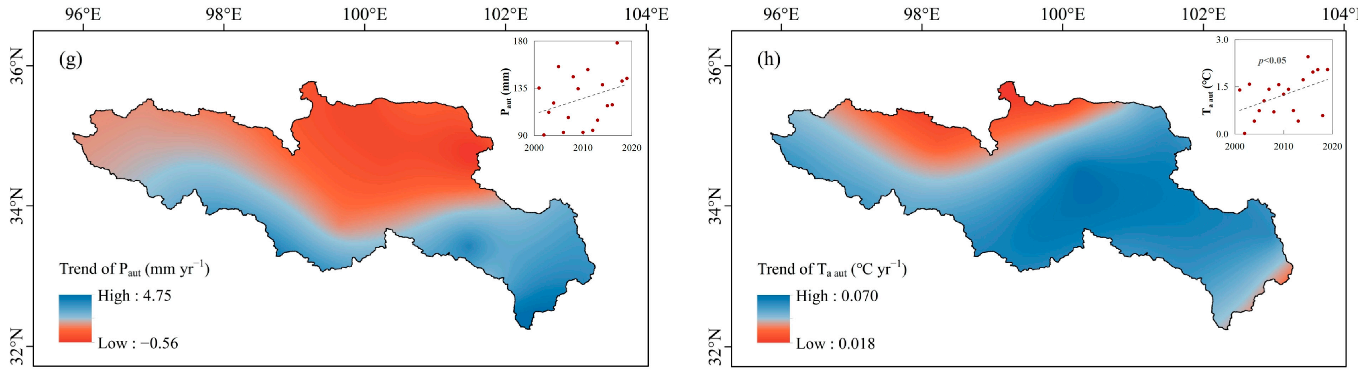

Figure 2. Spatial distribution of the trends of annual and seasonal precipitation and air temperature and their inter-annual variations in the SRYR from 2001 to 2019. (**a**) Annual precipitation (P), (**b**) annual air temperature (T_a), (**c**) spring precipitation (P_{spr}), (**d**) spring air temperature ($T_{a\ spr}$), (**e**) summer precipitation (P_{sum}), (**f**) summer air temperature ($T_{a\ sum}$), (**g**) autumn precipitation (P_{aut}) and (**h**) autumn air temperature ($T_{a\ aut}$). The inter-annual variations of annual and seasonal precipitation and air temperature in the SRYR from 2001 to 2019 are shown in the upper right corner.

3.2. Spatio-Temporal Variations of Vegetation Phenology

3.2.1. Spatial Variations

The spatial distribution of average vegetation phenology in the SRYR from 2001 to 2019 is shown in Figure 3. Four phenology factors (SOS, EOS, LOS and POS) exhibited obvious gradients from west to east. The average SOS gradually advanced from west to east (Figure 3a). Over the area, 82.5% of the pixels had a vegetation SOS in the range of 120–160 d from May to early June. The vegetation SOS was mostly concentrated in early and mid-June in the colder and drier western SRYR, while it was mostly concentrated in late April in the southeastern SRYR. By contrast, the average EOS was gradually delayed from west to east (Figure 3b). A total of 84.0% of the pixels had a vegetation EOS in the range of 270–300 d (October). The vegetation EOS was mostly less than 290 d in the western SRYR, while it was concentrated in 290–300 d (mid-to-late October) in the southeastern SRYR. The average LOS gradually extended from west to east (Figure 3c). The vegetation LOS was mostly less than 140 d in the western SRYR, while it was more than 160 d in the southeastern SRYR. The length of the vegetation growing season tended to extend under suitable hydrothermal conditions due to better activity from photosynthetic enzymes and soil microorganisms [58]. We observed that the longest LOS (>200 d) was in the southeastern SRYR. Similar to SOS, the average POS showed a pattern of delay from west to east (Figure 3d). The average POS mainly appeared in summer (June–August), and 86.5% of the pixels had a vegetation POS in the range of 200–220 d (late July to early August). The earliest POS (<190 d) was distributed in the southeastern SRYR where marsh was distributed.

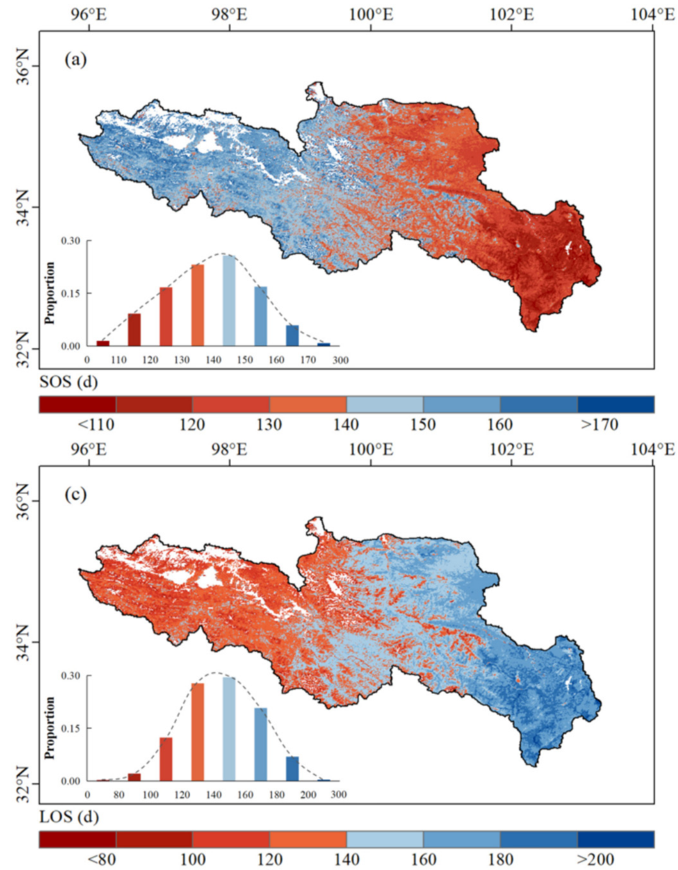

Figure 3. Spatial distribution of average vegetation: (**a**) SOS, (**b**) EOS, (**c**) LOS and (**d**) POS in the SRYR from 2001 to 2019. The frequency distribution of vegetation phenology is shown in the lower left corner.

3.2.2. Temporal Variations

The spatial distribution of the trends of vegetation phenology in the SRYR from 2001 to 2019 is shown in the Figure 4. The average SOS in the SRYR was 138.6 ± 3.6 d (Figure 4a) and showed a significantly advanced trend (-0.40 d yr^{-1}, $p < 0.01$). A total 25.2% of the SRYR had a significantly advanced SOS ($p < 0.05$), which was mainly distributed in the central and eastern SRYR. The average EOS in the region was 287.8 ± 2.6 d (Figure 4b) and showed a slightly and insignificantly advanced trend (-0.08 d yr^{-1}, $p > 0.05$). The average LOS in the SRYR was 149.2 ± 4.5 d (Figure 4c) and showed an insignificantly extended trend (+0.41 d yr^{-1}, $p > 0.05$). A total 18.0% of the SRYR had a significantly extended LOS ($p < 0.05$), which had a similar distribution pattern with that of the significantly advanced SOS. The extended LOS resulted from the advanced SOS in the central and eastern SRYR, which was consistent with the results of Zu et al. [59]. Shen et al. [60] found a significantly advanced SOS, delayed EOS and extended LOS in the Qinghai-Tibet Plateau. However, we did not find significant trends for EOS and LOS in the SRYR.

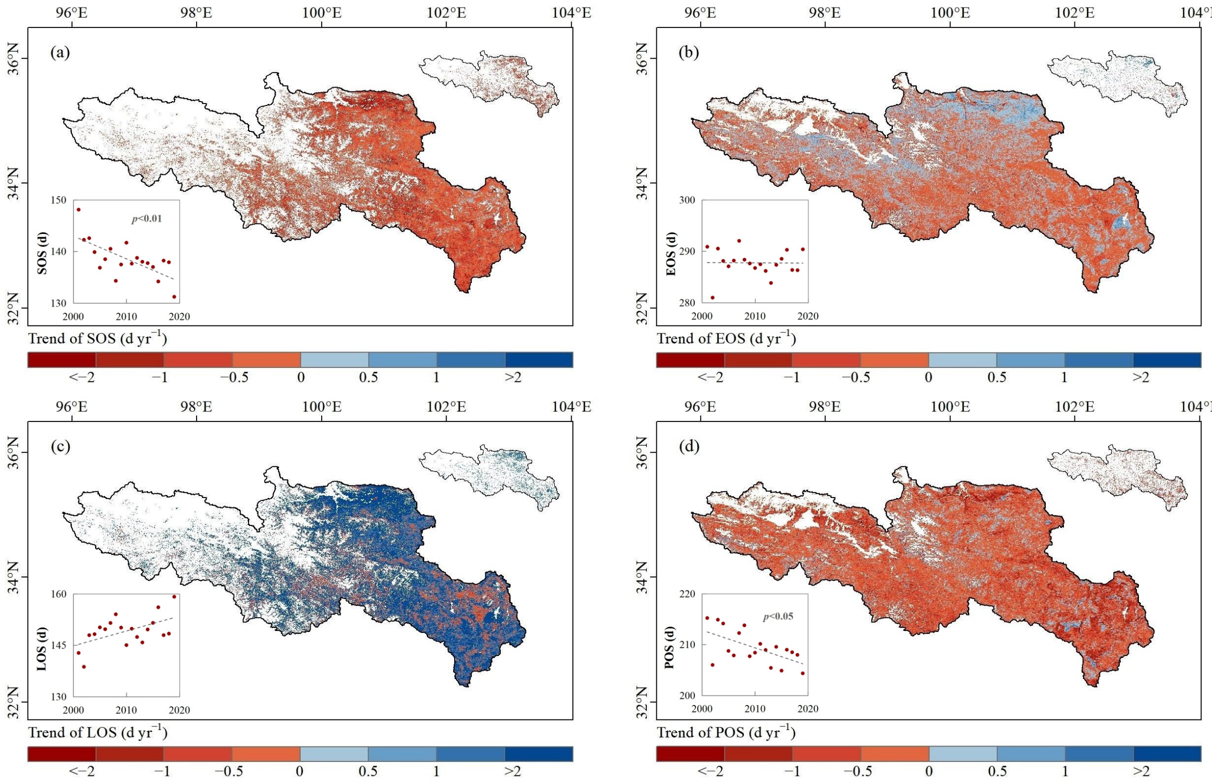

Figure 4. Spatial distribution of the trends of vegetation: (**a**) SOS, (**b**) EOS, (**c**) LOS and (**d**) POS in the SRYR from 2001 to 2019. The M-K test results of vegetation phenology are shown in the upper right corner, with red representing an advanced/extended trend and blue representing a delayed/shortened trend at a significance level of 0.05 (p < 0.05). The inter-annual variations of vegetation phenology in the SRYR from 2001 to 2019 are shown in the lower-left corner.

The average POS was 209.0 ± 3.3 d (Figure 4d) and showed a significantly advanced trend (−0.39 d yr^{-1}, p < 0.05). A total 19.1% of the pixels had a significantly advanced POS, while the proportion of regions in which the POS was significantly delayed (p < 0.05) was less than 1.0%. The regions with larger advanced rates (slope$_{POS}$ < 1.0 d yr^{-1}) were mainly distributed in the north, southeast and northwest of the SRYR.

3.3. Spatio-Temporal Variations of Seasonal GPP and Annual GPP

3.3.1. Spatial Variations

The spatial distribution of average annual GPP (GPP$_{ann}$) in the SRYR from 2001 to 2019 is shown in Figure 5a. The average GPP$_{ann}$ in the SRYR was 324.0 ± 24.4 g·C·m^{-2} and increased gradually from west to east. The region with a GPP$_{ann}$ less than 200 g·C·m^{-2} was primarily in the western SRYR, while that with more than 600.0 g·C·m^{-2} was primarily in the eastern SRYR. The average GPP$_{max}$ in the SRYR was 4.5 ± 0.5 g·C·m^{-2} and shared a similar spatial pattern with the average GPP$_{ann}$ (Figure 5b). The annual GPP$_{max}$ mainly occurred during the period from July to August, with the higher GPP$_{max}$ (>7.0 g·C·m^{-2}) in the eastern SRYR. The average annual values of spring GPP (GPP$_{spr}$) (Figure 5c), summer GPP (GPP$_{sum}$) (Figure 5d) and autumn GPP (GPP$_{aut}$) (Figure 5e) were, respectively, 28.1 ± 3.8 g·C·m^{-2}, 235.9 ± 24.0 g·C·m^{-2} and 59.9 ± 5.8 g·C·m^{-2}, and shared similar spatial patterns with GPP$_{ann}$ and GPP$_{max}$. As the average proportion of GPP$_{sum}$ to GPP$_{ann}$ reached 72.8%, GPP$_{sum}$ played an important role in regulating the spatio-temporal variations of GPP$_{ann}$. The average winter GPP (GPP$_{win}$) was close to 0 g·C·m^{-2} and could be neglected (Figure 5f), and thus GPP$_{win}$ was not further analyzed in this study.

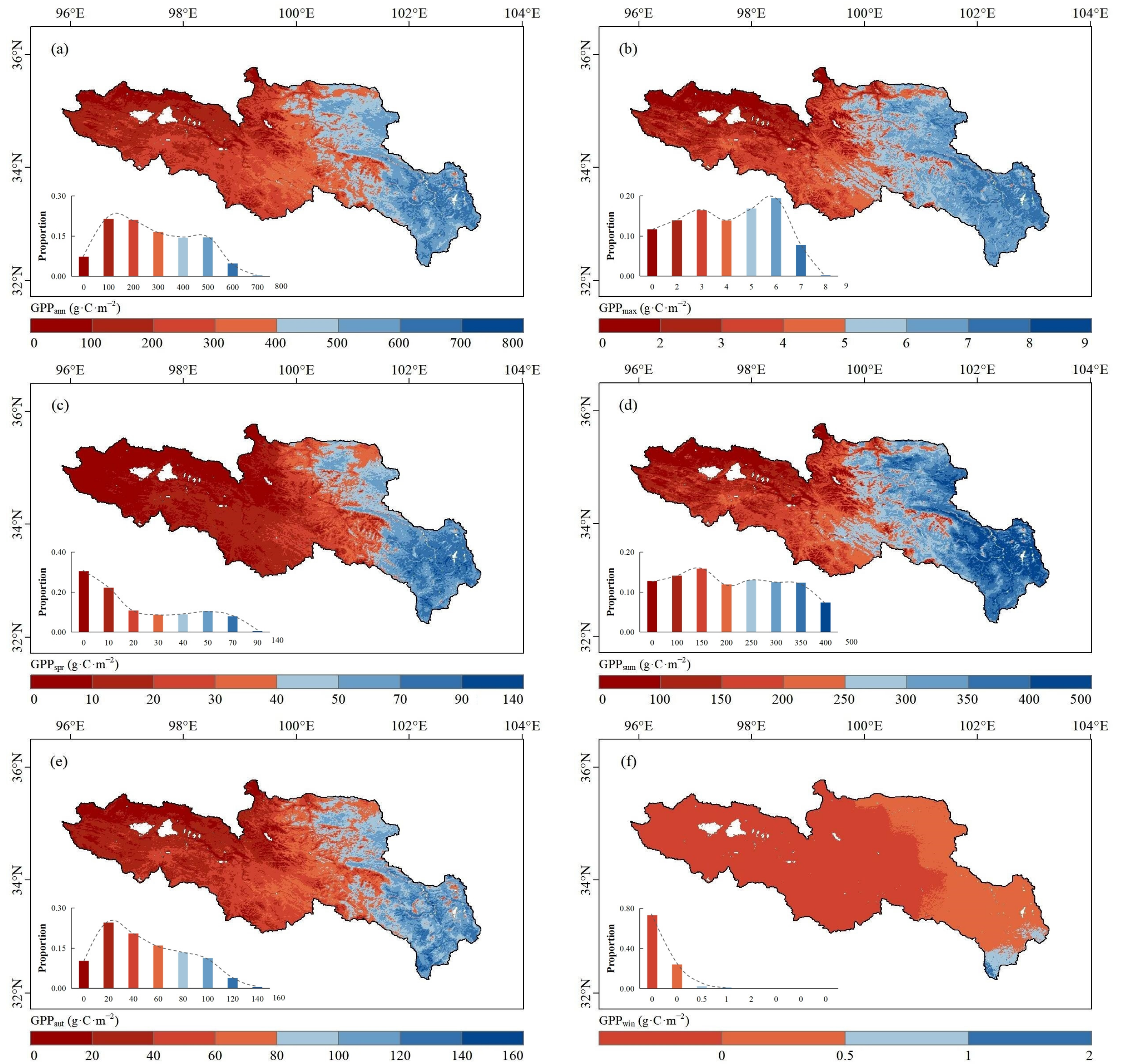

Figure 5. Spatial distribution of (**a**) average GPP_{ann}, (**b**) GPP_{max}, (**c**) GPP_{spr}, (**d**) GPP_{sum}, (**e**) GPP_{aut} and (**f**) GPP_{win} in the SRYR from 2001 to 2019. The frequency distribution of vegetation phenology is shown in the lower left corner.

3.3.2. Temporal Variations

The spatial distribution of the trends of GPP_{ann} and GPP_{max} in the SRYR from 2001 to 2019 are shown in Figures 6a and 6b. The GPP_{ann} and GPP_{max} in the SRYR both showed insignificantly increasing trends ($p > 0.05$), with rates of 1.76 g·C·m^{-2}·yr^{-1} and 0.03 g·C·m^{-2}·yr^{-1}, respectively. The significantly increasing GPP_{ann} and GPP_{max} ($p < 0.05$) accounted for 28.2% and 14.5% of the SRYR, respectively, and were mainly distributed in the west and north. A total 13.5% of the pixels had a decreasing GPP_{ann}, which was mainly distributed in the central SRYR.

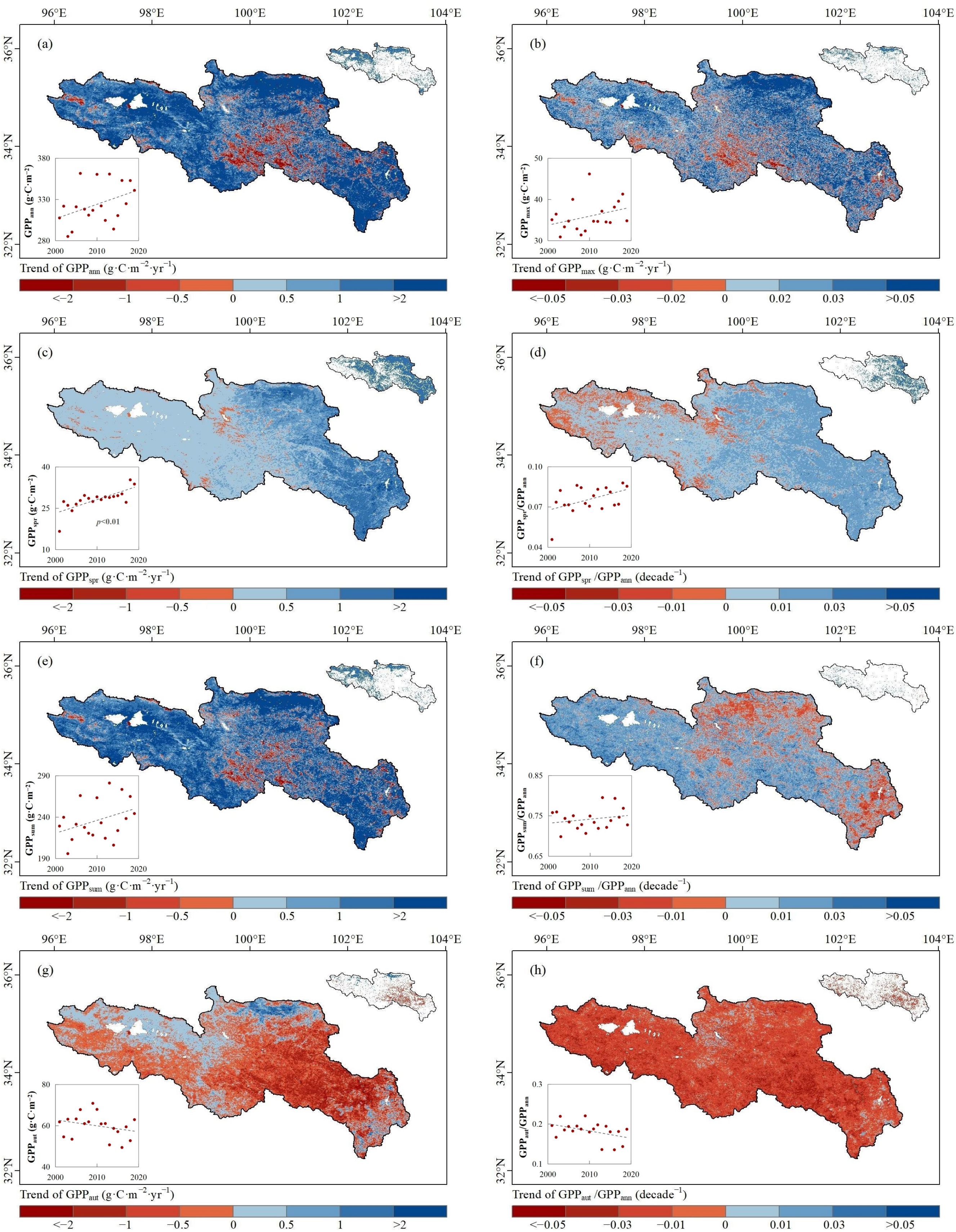

Figure 6. Spatial distribution of the trends of (**a**) annual GPP$_{ann}$, (**b**) GPP$_{max}$, (**c**) GPP$_{spr}$, (**d**) GPP$_{spr}$/GPP$_{ann}$, (**e**) GPP$_{sum}$, (**f**) GPP$_{sum}$/GPP$_{ann}$, (**g**) GPP$_{aut}$ and (**h**) GPP$_{aut}$/GPP$_{ann}$ in the SRYR

from 2001 to 2019. The trend with 0.05 significance level ($p < 0.05$) is shown in the upper right corner, with red representing a decreasing trend and blue representing an increasing trend at a significance level of 0.05 ($p < 0.05$), and the inter-annual variation is shown in the lower left corner.

GPP_{spr} exhibited a significantly increasing trend ($p < 0.01$) with a rate of 0.36 $g{\cdot}C{\cdot}m^{-2}{\cdot}yr^{-1}$ (Figure 6c). Most areas of the SRYR (96.2%) showed increasing GPP_{spr}, and areas with a significantly increasing trend reached 55.9% of the SRYR. GPP_{sum} exhibited an insignificantly increasing trend (+1.37 $g{\cdot}C{\cdot}m^{-2}{\cdot}yr^{-1}$, $p > 0.05$), and areas with a significantly increasing trend ($p < 0.05$) were 24.1% of the SRYR, which shared a similar distribution with the significantly increasing GPP_{ann} (Figure 6e). GPP_{aut} showed an insignificantly decreasing trend (−0.32 $g{\cdot}C{\cdot}m^{-2}{\cdot}yr^{-1}$, $p > 0.05$) and had spatial heterogeneities (Figure 6g). GPP_{aut} increased in the region where the EOS was delayed (Figure 4b) while it decreased in the region where the EOS advanced.

The results also indicated that the proportions of GPP_{spr} (Figure 6d) and GPP_{sum} to GPP_{ann} (Figure 6f) in the SRYR both experienced insignificantly increasing trends ($p > 0.05$), while the proportion of GPP_{aut} to GPP_{ann} (Figure 6h) showed an insignificantly decreasing trend ($p > 0.05$). This indicated that the contribution of spring and summer GPP to annual GPP was increasing and that of autumn GPP was decreasing.

3.4. Relationships between Seasonal GPP and Annual GPP

Table 2 illustrates six main change patterns of seasonal GPP and annual GPP in the SRYR. The dominant pattern was type I (51.79%) followed by type II (32.32%), indicating that most of the region (84.11%) had increasing GPP_{spr}, GPP_{sum} and GPP_{ann}. The main change pattern with decreasing GPP_{ann} was type III (7.75%) followed by type IV (3.48%). Though GPP_{spr} showed increasing trends both for type III and IV, GPP_{ann} showed decreasing trends due to either decreasing GPP_{sum} or GPP_{aut}. It was found that the trend of GPP_{ann} was strongly dependent on that of GPP_{sum}, because 94.1% of the pixels in the SRYR showed the same trends between GPP_{sum} and GPP_{ann}. As the photosynthetic activities in spring and autumn were constrained by low temperature in the SRYR, the annual GPP was mainly determined by GPP_{sum}.

Table 2. Six main patterns of the trends of annual and seasonal GPP in the SRYR from 2001 to 2019. "+" indicates an increasing trend while "−" indicates a decreasing trend.

Pattern	GPP_{ann}	GPP_{spr}	GPP_{sum}	GPP_{aut}	Area Proportion
I	+	+	+	−	51.79%
II	+	+	+	+	32.32%
III	−	+	−	−	7.75%
IV	−	+	+	−	3.48%
V	+	−	+	−	1.31%
VI	+	−	+	+	0.93%

3.5. Relationships among Climate, Phenology and GPP

3.5.1. Responses of Phenology and GPP_{max} to Seasonal Precipitation and Air Temperature

Figure 7 illustrates the Pearson correlation coefficients between vegetation phenology and GPP_{max} and their corresponding seasonal precipitation and air temperature in the SRYR from 2001 to 2019. We found that seasonal temperature had a stronger influence on SOS, EOS, POS and GPP_{max} than seasonal precipitation did. Each phenological factor had a significant correlation with the air temperature in their corresponding season in the SRYR. For example, spring phenology (SOS) was significantly and negatively correlated to average spring air temperature ($p < 0.05$). The increasing spring air temperature could stimulate photosynthetic activities and promote vegetation growth from the cold environment [13,61]. The spring phenology in the northeastern Tibetan Plateau was strongly advanced by increasing temperature and slightly advanced by precipitation, which is consistent with our results [62].

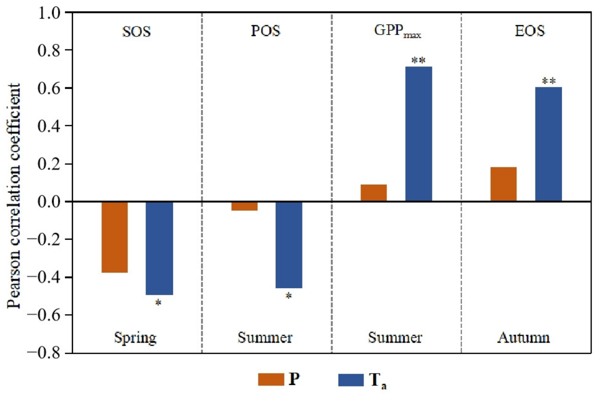

Figure 7. Pearson correlation coefficients between vegetation phenology and GPP_{max} and their corresponding seasonal precipitation (P) and air temperature (T_a). The asterisk on the bar chart indicates the level of significance. Single asterisk ("*") indicates statistically significant correlation coefficients with $p < 0.05$, and double asterisks ("**") indicate $p < 0.01$.

Autumn phenology (EOS) was significantly and positively correlated with autumn temperature ($p < 0.05$). The increasing autumn temperature enhanced the photosynthetic activities and decelerated chlorophyll degradation during leaf senescence processes [63,64]. In addition, increasing autumn temperature delayed the occurrence time of first frost and reduced the impacts of it on EOS [35,65]. However, EOS showed an insignificantly advancing trend, although autumn temperature showed a significantly increasing trend ($p < 0.05$) (Figure 2h), which might result from the stronger impacts of other factors, such as spring and summer phenology, on soil water and nutrients in autumn.

Summer phenology (POS) had a significantly negative correlation with summer temperature ($p < 0.05$). The results also showed that GPP_{max} had a significantly positive correlation with summer temperature ($p < 0.01$), consistent with the study conducted on the QTP [23], which found that GPP_{max} was dominated by temperature rather than precipitation in most regions of the QTP.

3.5.2. Responses of Seasonal and Annual GPP to Phenology Changes

Figure 8a shows the Pearson correlation coefficients of seasonal and annual GPP with phenology factors and GPP_{max} in the SRYR from 2001 to 2019. We found negative correlations between spring-summer phenology indicators and the corresponding seasonal GPP and a positive correlation between GPP_{max} and summer GPP, indicating that advanced SOS and POS and increasing GPP_{max} all enhanced the corresponding seasonal GPP. GPP_{spr} was significantly and negatively correlated to SOS ($p < 0.01$), and a one-day advance of SOS increased GPP_{spr} by 0.75 $g \cdot C \cdot m^{-2}$. GPP_{sum} was significantly and negatively correlated to POS ($p < 0.05$), and a one-day advance of POS increased GPP_{sum} by 3.73 $g \cdot C \cdot m^{-2}$. GPP_{sum} had a larger rate increase (> 2.0 $g \cdot C \cdot m^{-2}\ yr^{-1}$) (Figure 6e) in the north and southeast where POS had a larger rate advance (< -1.0 d yr^{-1}) (Figure 4d). Autumn GPP had weaker relationships with each phenology factor.

Due to the fact that average GPP_{sum} accounted for more than 70.0% of average GPP_{ann} in the SRYR, the advanced POS had a stronger impact on GPP_{ann} than SOS and EOS, and hence POS was significantly and negatively correlated to GPP_{ann} ($p < 0.05$) (Figure 8a). A one-day advance of POS increased GPP_{ann} by 4.23 $g \cdot C \cdot m^{-2}$. GPP_{max} had significant and positive correlations with GPP_{sum} ($p < 0.01$) and GPP_{ann} ($p < 0.01$), indicating that a greater GPP_{max} leads to a larger GPP_{sum} and GPP_{ann}. Moreover, GPP_{ann} had a stronger correlation (r = 0.765) with GPP_{max} than every phenology factor.

We also found a significant correlation between SOS and GPP_{spr}/GPP_{ann} ($p < 0.05$) (Figure 8b), indicating that an earlier SOS resulted in a larger contribution of spring GPP to annual GPP. The correlations between POS and GPP_{sum}/GPP_{ann} and between EOS and GPP_{aut}/GPP_{ann} were not significant. Moreover, there was no significant correlation between GPP_{max} and each phenology factor.

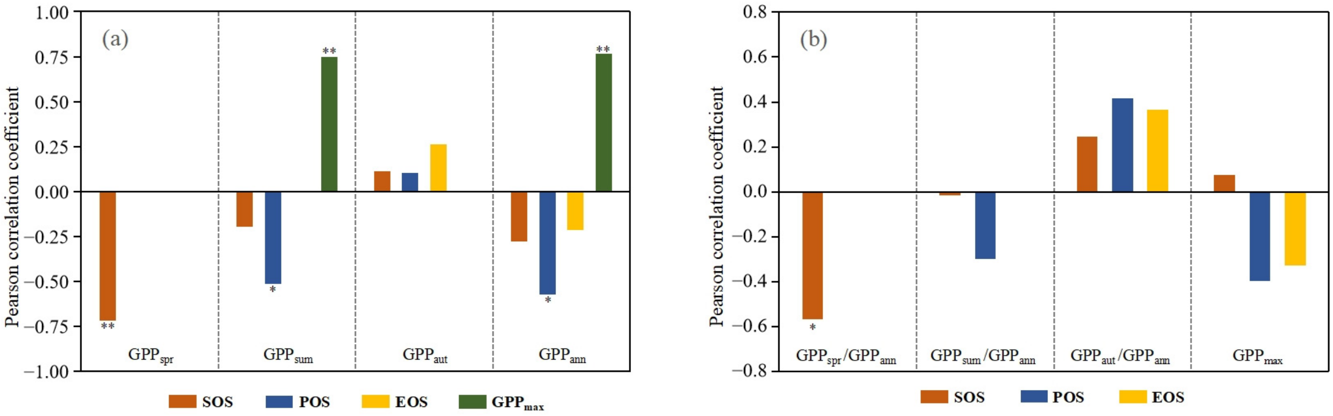

Figure 8. Pearson correlation coefficients of seasonal and annual GPP with phenology factors and GPP_{max} (**a**) and those of GPP_{spr}/GPP_{ann}, GPP_{sum}/GPP_{ann}, GPP_{aut}/GPP_{ann} and GPP_{max} with phenology factors (**b**). The asterisk on the bar chart indicates the level of significance. Single asterisk ("*") indicates statistically significant correlation coefficients with $p < 0.05$ and double asterisks ("**") indicate $p < 0.01$.

4. Discussion

4.1. Impacts of Phenology and Photosynthetic Capacity on Seasonal GPP

Previous studies found most of the QPT experienced increasing trends in vegetation productivity with the advancing of SOS, delaying of EOS and prolonging of LOS for the alpine grasslands [22,66]. In this study, advanced SOS and EOS and prolonged LOS were found in the SRYR from 2001 to 2019, which was consistent with the results from previous studies [22,67,68] in the QPT. Moreover, POS also showed a significantly advanced trend, which was seldom considered in the previous studies in the QTP. To clearly understand the impacts of phenology and photosynthetic capacity on seasonal GPP, we divided the study period into two periods: Period 1 (2001–2009) and Period 2 (2010–2019). Comparisons of the average daily GPP processes over growing season and the average values of vegetation phenology for Period 1 and Period 2 are shown in Figure 9a. Compared to Period 1, the average SOS, POS and EOS during Period 2 advanced 2.81 d, 3.47 d and 0.85 d, respectively, and the average LOS was extended 1.96 d. The average GPP_{spr}, GPP_{sum}, GPP_{ann} and GPP_{max} increased, respectively, 15.52%, 7.71%, 5.59% and 11.85%, while the average GPP_{aut} decreased 6.29%. The earlier SOS and POS might result in a greater consumption of soil-water and nutrients from plants in the spring and summer and limitations of soil-water and nutrients in the autumn. The alpine ecosystems in the SRYR exhibited an extended GPP curve in the growing season, an advanced peak in the growing season, and increased maximum carbon uptake capacity.

A conceptual figure indicating the influences of the changes of vegetation phenology and GPP_{max} on annual accumulative GPP is shown in Figure 9b. Changes in hydrothermal factors induce seasonal variation in the physiological activities of the vegetation, and hence contribute to the seasonal variability of vegetation productivity [69]. In this study, it was found that an advanced SOS prolonged the length of photosynthetic activity in spring in the SRYR. Moreover, an earlier spring phenology might result in greater leaf area, enhancing light interception and photosynthesis and thereby increased spring GPP [70]. Previous studies reported that an earlier spring phenology resulted in a longer growing season and strengthened productivity [21,23]. However, an earlier spring phenology could also result in soil moisture deficits by increasing water consumption [46,71], leading to suppressed vegetation activities in summer and autumn due to aggravated water stress for the water-limited grassland ecosystems [66,71].

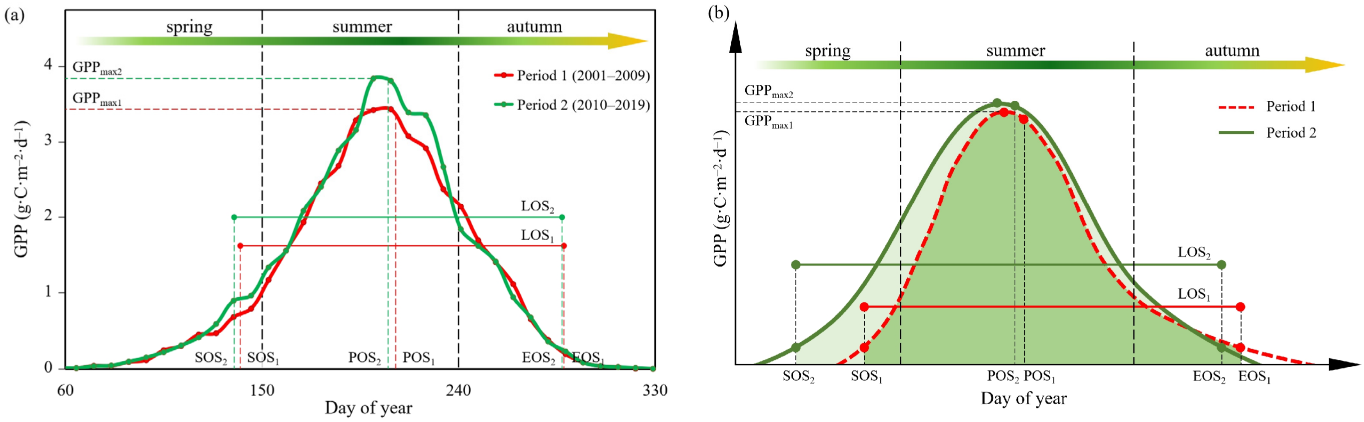

Figure 9. Comparison between annual cumulative gross primary productivities in the SRYR during Period 1 (2001–2009) and during Period 2 (2010–2019) (**a**). Conceptual figure indicating the influences of the changes of vegetation phenology and GPP_{max} on annual accumulative GPP (**b**). SOS_1, EOS_1, LOS_1, POS_1 and GPP_{max1} are the average values of phenology indicators and maximum GPP during Period 1, and SOS_2, EOS_2, LOS_2, POS_2 and GPP_{max2} are those during Period 2.

In this study, we found an earlier POS and higher GPP_{max} in the SRYR, both of which had positive effects on the GPP_{sum} and GPP_{ann}. Previous studies found that POS is an important vegetation phenology for the carbon cycle of terrestrial ecosystems [27], and an advance of POS could result in productivity changes [72]. Researchers found an earlier POS shifted towards spring in the Northern Hemisphere, caused by climate warming, resulted in increased vegetation productivity [44,73]. We found the spatial patterns of the regions with significantly increased GPP_{max} (Figure 6b) were similar to those with significantly advanced POS (Figure 4d) in the SRYR. Moreover, both POS and GPP_{max} had significant correlations to summer GPP (Figure 8a). Therefore, it is suggested that an earlier POS and higher GPP_{max} increased GPP_{sum} by promoting vegetation photosynthesis [27,72], further resulting in an increased GPP_{ann}. As shown in Figure 9a, the increase of GPP_{max} ($GPP_{max2} > GPP_{max1}$) had important contributions to the increase of summer GPP and reshaped the cumulative curve of annual GPP with vegetation phenology.

4.2. POS and the Timing of GPP_{max}

It is worth noting that the POS in this study corresponded to the maximal vegetation index, which represents the timing of the seasonal peak canopy structure, and did not match with the timing of GPP_{max}. Ge et al. [74] found that the seasonal peak for photosynthesis was earlier than the peak for canopy structure in more than 87.5% of the ecosystems in the Northern Hemisphere (>30°N), and this mismatch increased due to increasing atmospheric CO_2. The timing of GPP_{max} is important to characterize seasonal carbon uptake [75]. GPP_{max} is not only affected by canopy structure but also affected by light use efficiency, which is regulated by environmental conditions, and the potential maximum GPP_{max} is achieved when the densest canopy matches the ideal resource availability [68]. We found the timings of GPP_{max} were about 2.2 d and 6.7 d earlier than the POS for Period 1 and Period 2 in the SRYR, respectively.

4.3. Uncertainty

In this study, we used the vegetation phenology and productivity datasets from MODIS products to investigate the dynamics of vegetation phenology and GPP. It should be noted that uncertainty existed in remote sensing products due to the flaws of the model structures and input parameters. For example, MCD12Q2 was derived by using the threshold method based on the vegetation index data series, and the given threshold was set to extract the vegetation phenology. However, the selection of the threshold is often arbitrarily determined and could induce uncertainty [22,76,77]. In addition, the sparse temporal resolutions (e.g., 8 days for MODIS EVI) of satellite data might lead to limitations in capturing the accurate dynamics of vegetation phenology [78]. In the estimation of GPP, uncertainties were from climate input and the determination of maximum light use efficiency (LUE) for vegetation, which was influenced by land cover types, phenophases and environmental stresses [79,80]. Due to the lack of ground observation, the performance of these remote sensing products on vegetation phenology and gross primary productivity was not evaluated in this study.

This study analyzed the correlation between seasonal GPP and phenological factors, but the separate contributions of the changes of phenology factors and GPP_{max} to seasonal and annual GPP were not quantified. In recent years, global scale solar-induced chlorophyll fluorescence (SIF) provides a better surrogate for studies of large-scale vegetation phenology and GPP [81,82]. The study of phenology monitoring by SIF remote sensing may lead to further discoveries on the influence of phenology on vegetation photosynthesis and carbon sequestration in the source region of the Yellow River. Moreover, vegetation phenology was affected not only by precipitation and air temperature, but also by radiation, grazing, snowmelt and permafrost degradation and phenology and productivity in the preceding year [29,83–86]. We only considered the impacts of precipitation and air temperature on vegetation phenology in this paper. Besides vegetation phenology and GPP_{max}, other environmental factors such as atmospheric CO_2 concentrations, grazing, vapor pressure deficits and radiation also affected carbon assimilation. In further studies quantifying the impacts of vegetation phenology on productivity, these uncertainties should be taken into accounted, and the underlying mechanisms need to be further explored.

5. Conclusions

This study examined the spatio-temporal variations of vegetation phenology and GPP at seasonal and annual scales in the SRYR using 19-year remote sensing data and explored the impacts of vegetation phenology and photosynthetic carbon uptake capacity on seasonal and annual GPP. We found that not only spring phenology (SOS) but also summer phenology (POS) significantly advanced in the SRYR. The start (SOS) and peak (POS) of the growing season from 2001 to 2019 experienced significantly advanced trends ($p < 0.05$) at rates of 0.41 d yr^{-1} and 0.39 d yr^{-1}, respectively. The increased spring and summer air temperatures were the dominant climate factors for the advanced SOS and POS, respectively. Spring GPP showed a significantly increasing trend ($p < 0.01$) at a rate of 0.50 $g \cdot C \cdot m^{-2} \cdot yr^{-1}$, and the earlier SOS had obvious positive effects on GPP_{spr}, with a one-day advance in SOS increasing GPP_{spr} by 0.75 $g \cdot C \cdot m^{-2}$. Summer GPP was significantly and negatively correlated to POS ($p < 0.05$), and a one-day advance in POS increased GPP_{sum} by 3.73 $g \cdot C \cdot m^{-2}$. Earlier start and peak of growing season had significantly positive effects on spring GPP and summer GPP, respectively. Moreover, maximum carbon uptake capacity (GPP_{max}) had significant and positive correlations with GPP_{sum} and GPP_{ann} ($p < 0.01$). It was found that earlier an spring-summer phenology and higher photosynthetic peak altered the seasonal patterns of vegetation productivity in the SRYR. Most of the existing studies focused on the effects of spring and autumn phenology on annual productivity in the QPT. The main objective of this study was to explore the effects of vegetation phenology, including peak greenness timing (POS) and photosynthetic capacity on seasonal GPP. This study suggested that not only spring and autumn phenology but also summer phenology and maximum carbon uptake capacity should be regarded as crucial indicators regulating the carbon uptake process in alpine ecosystems. This research provides important information about the response characteristics of ecosystem productivity to phenology changes for alpine ecosystems under global climate warming. Further studies are still needed to assess and reduce the uncertainty associated with the remote sensing phenology and productivity products.

Author Contributions: Conceptualization, F.Y. and T.L.; methodology, F.Y., C.L., Q.C. and J.L.; formal analysis, F.Y. and Q.C.; writing—original draft preparation, F.Y.; writing—review and editing, C.L.,

J.L. and T.L.; funding acquisition, T.L. All authors have read and agreed to the published version of the manuscript.

Funding: This work is supported by National Natural Sciences Foundation of China (No. 42071038).

Data Availability Statement: Data are contained within the article.

Acknowledgments: We thank the Land Processes Distributed Active Archive Center for providing MODIS satellite data. We thank the China Meteorological Data Service Center for providing meteorological data.

Conflicts of Interest: The authors declare no conflicts of interest.

Abbreviations

SOS—start of growing season; EOS—end of growing season; POS—peak of growing season; LOS—length of growing season; GPP—gross primary productivity; GPP_{max}—maximum carbon uptake capacity; GPP_{spr}—spring GPP; GPP_{sum}—summer GPP; GPP_{aut}—autumn GPP; GPP_{ann}—annual GPP; LUE—light use efficiency; P—precipitation; T_a—air temperature; P_{spr}—spring precipitation; P_{sum}—summer precipitation; P_{aut}—autumn precipitation; $T_{a\ spr}$—spring air temperature; $T_{a\ sum}$—summer air temperature; $T_{a\ aut}$—autumn air temperature; SRYR—source region of the Yellow River; QTP—Qinghai-Tibet Plateau; NASA—National Aeronautics and Space Administration; EVI—Enhanced Vegetation Index; BRDF—bidirectional reflectance distribution function; DEM—digital elevation model; SIF—solar-induced chlorophyll fluorescence; MVC—maximum value composite.

References

1. Anav, A.; Friedlingstein, P.; Beer, C.; Ciais, P.; Harper, A.; Jones, C.; Murray-Tortarolo, G.; Papale, D.; Parazoo, N.C.; Peylin, P.; et al. Spatiotemporal patterns of terrestrial gross primary production: A review. *Rev. Geophys.* **2015**, *53*, 785–818. [CrossRef]
2. Yao, Y.T.; Wang, X.H.; Li, Y.; Wang, T.; Shen, M.G.; Du, M.Y.; He, H.L.; Li, Y.N.; Luo, W.J.; Ma, M.G.; et al. Spatiotemporal pattern of gross primary productivity and its covariation with climate in China over the last thirty years. *Glob. Chang. Biol.* **2018**, *24*, 184–196. [CrossRef] [PubMed]
3. Xia, J.Y.; Niu, S.L.; Ciais, P.; Janssens, I.A.; Chen, J.Q.; Ammann, C.; Arain, A.; Blanken, P.D.; Cescatti, A.; Bonal, D.; et al. Joint control of terrestrial gross primary productivity by plant phenology and physiology. *Proc. Natl. Acad. Sci. USA* **2015**, *112*, 2788–2793. [CrossRef] [PubMed]
4. Zhou, S.; Zhang, Y.; Caylor, K.K.; Luo, Y.Q.; Xiao, X.M.; Ciais, P.; Huang, Y.F.; Wang, G.Q. Explaining inter-annual variability of gross primary productivity from plant phenology and physiology. *Agric. For. Meteorol.* **2016**, *226*, 246–256. [CrossRef]
5. Running, S.W.; Nemani, R.R.; Heinsch, F.A.; Zhao, M.S.; Reeves, M.; Hashimoto, H. A continuous satellite-derived measure of global terrestrial primary production. *AIBS Bull.* **2004**, *54*, 547–560. [CrossRef]
6. Richardson, A.D.; Keenan, T.F.; Migliavacca, M.; Ryu, Y.; Sonnentag, O.; Toomey, M. Climate change, phenology, and phenological control of vegetation feedbacks to the climate system. *Agric. For. Meteorol.* **2013**, *169*, 156–173. [CrossRef]
7. Wu, C.Y.; Hou, X.H.; Peng, D.L.; Gonsamo, A.; Xu, S.G. Land surface phenology of China's temperate ecosystems over 1999-2013: Spatial-temporal patterns, interaction effects, covariation with climate and implications for productivity. *Agric. For. Meteorol.* **2016**, *216*, 177–187. [CrossRef]
8. Yang, J.L.; Dong, J.W.; Xiao, X.M.; Dai, J.H.; Wu, C.Y.; Xia, J.Y.; Zhao, G.S.; Zhao, M.M.; Li, Z.L.; Zhang, Y.; et al. Divergent shifts in peak photosynthesis timing of temperate and alpine grasslands in China. Remote Sens. *Environ.* **2019**, *233*, 111395.
9. Luo, M.; Meng, F.H.; Sa, C.L.; Duan, Y.C.; Bao, Y.H.; Liu, T.; De Maeyer, P. Response of vegetation phenology to soil moisture dynamics in the Mongolian plateau. *Catena* **2021**, *206*, 105505. [CrossRef]
10. Zhang, T.; Tang, Y.Y.; Xu, M.J.; Zhao, G.; Chen, N.; Zheng, Z.T.; Zhu, J.T.; Ji, X.M.; Wang, D.F.; Zhang, Y.J.; et al. Joint control of alpine meadow productivity by plant phenology and photosynthetic capacity. *Agric. For. Meteorol.* **2022**, *325*, 109135. [CrossRef]
11. Falge, E.; Baldocchi, D.; Tenhunen, J.; Aubinet, M.; Bakwin, P.; Berbigier, P.; Bernhofer, C.; Burba, G.; Clement, R.; Davis, K.J.; et al. Seasonality of ecosystem respiration and gross primary production as derived from FLUXNET measurements. *Agric. For. Meteorol.* **2002**, *113*, 53–74. [CrossRef]
12. Zhang, W.K.; Yu, G.R.; Chen, Z.; Zhang, L.M.; Wang, Q.F.; Zhang, Y.J.; He, H.L.; Han, L.; Chen, S.P.; Han, S.J.; et al. Attribute parameter characterized the seasonal variation of gross primary productivity (αGPP): Spatiotemporal variation and influencing factors. *Agric. For. Meteorol.* **2020**, *280*, 107774. [CrossRef]
13. Zheng, Z.T.; Zhu, W.Q.; Zhang, Y.J. Seasonally and spatially varied controls of climatic factors on net primary productivity in alpine grasslands on the Tibetan Plateau. *Glob. Ecol. Conserv.* **2020**, *21*, e00814. [CrossRef]
14. Piao, S.L.; Ciais, P.; Friedlingstein, P.; Peylin, P.; Reichstein, M.; Luyssaert, S.; Margolis, H.; Fang, J.Y.; Barr, A.; Chen, A.P.; et al. Net carbon dioxide losses of northern ecosystems in response to autumn warming. *Nature* **2008**, *451*, 49–52. [CrossRef]

15. Buermann, W.; Forkel, M.; O'Sullivan, M.; Sitch, S.; Friedlingstein, P.; Haverd, V.; Jain, A.K.; Kato, E.; Kautz, M.; Lienert, S.; et al. Widespread seasonal compensation effects of spring warming on northern plant productivity. *Nature* **2018**, *562*, 110–115. [CrossRef]
16. Zani, D.; Crowther, T.W.; Mo, L.D.; Renner, S.S.; Zohner, C.M. Increased growing-season productivity drives earlier autumn leaf senescence in temperate trees. *Science* **2020**, *370*, 1066–1071. [CrossRef] [PubMed]
17. Yang, L.; Zhao, S.Q. A stronger advance of urban spring vegetation phenology narrows vegetation productivity difference between urban settings and natural environments. *Sci. Total Environ.* **2023**, *868*, 161649. [CrossRef]
18. Steltzer, H.; Post, E. Seasons and Life Cycles. *Science* **2009**, *324*, 886–887. [CrossRef] [PubMed]
19. Ren, S.L.; Peichl, M. Enhanced spatiotemporal heterogeneity and the climatic and biotic controls of autumn phenology in northern grasslands. *Sci. Total Environ.* **2021**, *788*, 147806. [CrossRef]
20. Fang, H.S.; Sha, M.Q.; Xie, Y.C.; Lin, W.J.; Qiu, D.; Tu, J.G.; Tan, X.C.; Li, X.L.; Sha, Z.Y. Shifted global vegetation phenology in response to climate changes and its feedback on vegetation carbon uptake. *Remote Sens.* **2023**, *15*, 2288. [CrossRef]
21. Cheng, M.; Jin, J.X.; Jiang, H. Strong impacts of autumn phenology on grassland ecosystem water use efficiency on the Tibetan Plateau. *Ecol. Indic.* **2021**, *126*, 107682. [CrossRef]
22. Wang, S.Y.; Zhang, B.; Yang, Q.C.; Chen, G.S.; Yang, B.J.; Lu, L.L.; Shen, M.; Peng, Y.Y. Responses of net primary productivity to phenological dynamics in the Tibetan Plateau, China. *Agric. For. Meteorol.* **2017**, *232*, 235–246. [CrossRef]
23. Chen, S.L.; Huang, Y.F.; Gao, S.; Wang, G.Q. Impact of physiological and phenological change on carbon uptake on the Tibetan Plateau revealed through GPP estimation based on spaceborne solar-induced fluorescence. *Sci. Total Environ.* **2019**, *663*, 45–59. [CrossRef] [PubMed]
24. Wilson, D. Variation in leaf respiration in relation to growth and photosynthesis of LOLIUM. *Ann. Appl. Biol.* **1975**, *80*, 323–338. [CrossRef]
25. Wu, C.Y.; Chen, J.M.; Gonsamo, A.; Price, D.T.; Black, T.A.; Kurz, W.A. Interannual variability of net carbon exchange is related to the lag between the end-dates of net carbon uptake and photosynthesis: Evidence from long records at two contrasting forest stands. *Agric. For. Meteorol.* **2012**, *164*, 29–38. [CrossRef]
26. Huang, K.; Xia, J.Y.; Wang, Y.P.; Ahlström, A.; Chen, J.Q.; Cook, R.B.; Cui, E.Q.; Fang, Y.Y.; Fisher, J.B.; Huntzinger, D.N.; et al. Enhanced peak growth of global vegetation and its key mechanisms. *Nat. Ecol. Evol.* **2018**, *2*, 1897–1905. [CrossRef] [PubMed]
27. Wang, X.Y.; Wu, C.Y. Estimating the peak of growing season (POS) of China's terrestrial ecosystems. *Agric. For. Meteorol.* **2019**, *278*, 107639. [CrossRef]
28. Musavi, T.; Migliavacca, M.; Reichstein, M.; Kattge, J.; Wirth, C.; Black, T.A.; Janssens, I.; Knohl, A.; Loustau, D.; Roupsard, O.; et al. Stand age and species richness dampen interannual variation of ecosystem-level photosynthetic capacity. *Nat. Ecol. Evol.* **2017**, *1*, 0048. [CrossRef]
29. Zhang, J.R.; Xiao, J.F.; Tong, X.J.; Zhang, J.S.; Meng, P.; Li, J.; Liu, P.R.; Yu, P.Y. NIRv and SIF better estimate phenology than NDVI and EVI: Effects of spring and autumn phenology on ecosystem production of planted forests. *Agric. For. Meteorol.* **2022**, *315*, 108819. [CrossRef]
30. Stoy, P.C.; Trowbridge, A.M.; Bauerle, W.L. Controls on seasonal patterns of maximum ecosystem carbon uptake and canopy-scale photosynthetic light response: Contributions from both temperature and photoperiod. *Photosynth. Res.* **2014**, *119*, 49–64. [CrossRef]
31. Zhu, J.T.; Zhang, Y.J.; Jiang, L. Experimental warming drives a seasonal shift of ecosystem carbon exchange in Tibetan alpine meadow. *Agric. For. Meteorol.* **2017**, *233*, 242–249. [CrossRef]
32. Wang, R.; Dong, Z.B.; Zhou, Z.C. Different responses of vegetation to frozen ground degradation in the source region of the Yellow River from 1980 to 2018. *Chin. Geogr. Sci.* **2020**, *30*, 557–571. [CrossRef]
33. Deng, M.S.; Meng, X.H.; Lu, Y.Q.; Shu, L.L.; Li, Z.G.; Zhao, L.; Chen, H.; Shang, L.Y.; Sheng, D.R.; Ao, X.M. Impact of climatic and vegetation dynamic change on runoff over the Three Rivers Source Region based on the Community Land Model. *Clim. Dyn.* **2023**, *61*, 1193–1208. [CrossRef]
34. Iqbal, M.; Wen, J.; Wang, S.P.; Tian, H.; Adnan, M. Variations of precipitation characteristics during the period 1960–2014 in the source region of the Yellow River, China. *J. Arid. Land* **2018**, *10*, 388–401. [CrossRef]
35. Li, S.S.; Gao, Y.H.; Lyu, S.H.; Liu, Y.P.; Pan, Y.J. Response of surface air temperature to the change of leaf area index in the source region of the Yellow River by the WRF model. *Theor. Appl. Climatol.* **2019**, *138*, 1755–1765. [CrossRef]
36. Jin, H.J.; He, R.X.; Cheng, G.D.; Wu, Q.B.; Wang, S.L.; Lu, L.Z.; Chang, X.L. Changes in frozen ground in the source area of the Yellow River on the Qinghai-Tibet Plateau, China, and their eco-environmental impacts. *Environ. Res. Lett.* **2009**, *4*, 045206. [CrossRef]
37. Wang, T.H.; Yang, D.W.; Qin, Y.; Wang, Y.H.; Chen, Y.; Gao, B.; Yang, H.B. Historical and future changes of frozen ground in the upper Yellow River Basin. *Glob. Planet. Chang.* **2018**, *162*, 199–211. [CrossRef]
38. Liu, X.Y.; Liu, C.; Fan, B.H.; Li, L.G.; Tan, B.; Jin, Z.W.; Lu, H.; Liu, T.G. Spatial responses of ecosystem water-use efficiency to hydrothermal and vegetative gradients in alpine grassland ecosystem in drylands. *Ecol. Indic.* **2022**, *141*, 109064. [CrossRef]
39. Xue, B.L.; Wang, L.; Li, X.P.; Yang, K.; Chen, D.L.; Sun, L.T. Evaluation of evapotranspiration estimates for two river basins on the Tibetan Plateau by a water balance method. *J. Hydrol.* **2013**, *492*, 290–297. [CrossRef]
40. Liu, J.; Chen, J.J.; Qin, Q.T.; You, H.T.; Han, X.W.; Zhou, G.Q. Patch pattern and ecological risk assessment of alpine grassland in the source region of the Yellow River. *Remote Sens.* **2020**, *12*, 3460. [CrossRef]

41. Jiang, Z.Y.; Huete, A.R.; Didan, K.; Miura, T. Development of a two-band enhanced vegetation index without a blue band. *Remote Sens. Environ.* **2008**, *112*, 3833–3845. [CrossRef]
42. Jia, W.X.; Zhao, S.Q.; Zhang, X.Y.; Liu, S.G.; Henebry, G.M.; Liu, L.L. Urbanization imprint on land surface phenology: The urban-rural gradient analysis for Chinese cities. *Glob. Chang. Biol.* **2021**, *27*, 2895–2904. [CrossRef]
43. Ren, S.L.; Vitasse, Y.; Chen, X.Q.; Peichl, M.; An, S. Assessing the relative importance of sunshine, temperature, precipitation, and spring phenology in regulating leaf senescence timing of herbaceous species in China. *Agric. For. Meteorol.* **2022**, *313*, 108770. [CrossRef]
44. Gonsamo, A.; Chen, J.M.; Ooi, Y.W. Peak season plant activity shift towards spring is reflected by increasing carbon uptake by extratropical ecosystems. *Glob. Chang. Biol.* **2018**, *24*, 2117–2128. [CrossRef]
45. Ji, Z.X.; Pei, T.T.; Chen, Y.; Wu, H.W.; Hou, Q.Q.; Shi, F.Z.; Xie, B.P.; Zhang, J.X. The driving factors of grassland water use efficiency along degradation gradients on the Qinghai-Tibet Plateau, China. *Glob. Ecol. Conserv.* **2022**, *35*, e02090. [CrossRef]
46. Lian, X.; Piao, S.L.; Li, L.Z.X.; Li, Y.; Huntingford, C.; Ciais, P.; Cescatti, A.; Janssens, I.A.; Penuelas, J.; Buermann, W.; et al. Summer soil drying exacerbated by earlier spring greening of northern vegetation. *Sci. Adv.* **2020**, *6*, eaax0255. [CrossRef]
47. Huang, K.; Zhang, Y.J.; Tagesson, T.; Brandt, M.; Wang, L.H.; Chen, N.; Zu, J.X.; Jin, H.X.; Cai, Z.Z.; Tong, X.W.; et al. The confounding effect of snow cover on assessing spring phenology from space: A new look at trends on the Tibetan Plateau. *Sci. Total Environ.* **2021**, *756*, 144011. [CrossRef] [PubMed]
48. Ma, D.J.; Wu, X.D.; Ma, X.L.; Wang, J.P.; Lin, X.W.; Mu, C.C. Spatial, phenological, and inter-Annual variations of gross primary productivity in the Arctic from 2001 to 2019. *Remote Sens.* **2021**, *13*, 2875. [CrossRef]
49. Wang, J.Y.; Sun, H.Z.; Xiong, J.N.; He, D.; Cheng, W.M.; Ye, C.C.; Yong, Z.W.; Huang, X.L. Dynamics and drivers of vegetation phenology in Three-River headwaters region based on the Google Earth Engine. *Remote Sens.* **2021**, *13*, 2528. [CrossRef]
50. Editorial Board of Vegetation Map of China; Chinese Academy of Sciences. *Vegetation Map of the People's Republic of China (1:1,000,000) (Digital Version)*; Geology Press: Beijing, China, 2007.
51. Holben, B.N. Characteristics of maximum-value composite images from temporal AVHRR data. *Int. J. Remote Sens.* **1986**, *7*, 1417–1434. [CrossRef]
52. Environmental Systems Research Institute (ESRI). *ArcGIS Desktop: Release 10.6*; Environmental Systems Research Institute (ESRI): Redlands, CA, USA, 2018; Available online: https://www.esri.com (accessed on 20 January 2020).
53. Sen, P.K. Estimates of the regression coeffcient based on Kendall's tau. *J. Am. Stat. Assoc.* **1968**, *63*, 1379–1389. [CrossRef]
54. Mann, H.B. Nonparametric tests against trend. *Econometrica* **1945**, *13*, 245–259. [CrossRef]
55. Kendall, M.G. *Rank Correlation Measures*; Charles Griffin: London, UK, 1975.
56. The MathWorks, Inc. *MATLAB*, Version 2018b; The MathWorks, Inc.: Natick, MA, USA, 2018. Available online: https://www.mathworks.com (accessed on 4 February 2020).
57. Zhang, J.R.; Gonsamo, A.; Tong, X.J.; Xiao, J.F.; Rogers, C.A.; Qin, S.H.; Liu, P.R.; Yu, P.Y.; Ma, P. Solar-induced chlorophyll fluorescence captures photosynthetic phenology better than traditional vegetation indices. *ISPRS J. Photogramm. Remote Sens.* **2023**, *203*, 183–198. [CrossRef]
58. Sun, H.Z.; Chen, Y.B.; Xiong, J.N.; Ye, C.H.; Yong, Z.W.; Wang, Y.; He, D.; Xu, S.C. Relationships between climate change, phenology, edaphic factors, and net primary productivity across the Tibetan Plateau. *Int. J. Appl. Earth Obs. Geoinf.* **2022**, *107*, 102708. [CrossRef]
59. Zu, J.X.; Zhang, Y.J.; Huang, K.; Liu, Y.J.; Chen, N.; Cong, N. Biological and climate factors co-regulated spatial-temporal dynamics of vegetation autumn phenology on the Tibetan Plateau. *Int. J. Appl. Earth Obs. Geoinf.* **2018**, *69*, 198–205. [CrossRef]
60. Shen, M.G.; Wang, S.P.; Jiang, N.; Sun, J.P.; Cao, R.Y.; Ling, X.F.; Fang, B.; Zhang, L.; Zhang, L.H.; Xu, X.Y.; et al. Plant phenology changes and drivers on the Qinghai-Tibetan Plateau. *Nat. Rev. Earth Environ.* **2022**, *3*, 633–651. [CrossRef]
61. Shen, X.J.; Xue, Z.S.; Jiang, M.; Lu, X.G. Spatiotemporal change of vegetation coverage and its Relationship with climate change in freshwater marshes of northeast China. *Wetlands* **2019**, *39*, 429–439. [CrossRef]
62. Cheng, M.; Wang, Y.; Zhu, J.X.; Pan, Y. Precipitation dominates the relative contributions of climate factors to grasslands spring phenology on the Tibetan Plateau. *Remote Sens.* **2022**, *14*, 517. [CrossRef]
63. Shi, C.G.; Sun, G.; Zhang, H.X.; Xiao, B.X.; Ze, B.; Zhang, N.N.; Wu, N. Effects of warming on chlorophyll degradation and carbohydrate accumulation of alpine herbaceous species during plant senescence on the Tibetan Plateau. *PLoS ONE* **2014**, *9*, e107874. [CrossRef] [PubMed]
64. Liu, Q.; Fu, Y.S.H.; Zeng, Z.Z.; Huang, M.T.; Li, X.R.; Piao, S.L. Temperature, precipitation, and insolation effects on autumn vegetation phenology in temperate China. *Glob. Chang. Biol.* **2016**, *22*, 644–655. [CrossRef] [PubMed]
65. Gill, A.L.; Gallinat, A.S.; Sanders-DeMott, R.; Rigden, A.J.; Gianotti, D.J.S.; Mantooth, J.A.; Templer, P.H. Changes in autumn senescence in northern hemisphere deciduous trees: A meta-analysis of autumn phenology studies. *Ann. Bot.* **2015**, *116*, 875–888. [CrossRef]
66. Zheng, Z.T.; Zhu, W.Q.; Zhang, Y.J. Direct and lagged effects of spring phenology on net primary productivity in the alpine grasslands on the Tibetan Plateau. *Remote Sens.* **2020**, *12*, 1223. [CrossRef]
67. Li, X.Y.; Zhao, C.Z.; Kang, M.P.; Ma, M. Responses of net primary productivity to phenological dynamics based on a data fusion algorithm in the northern Qinghai-Tibet Plateau. *Ecol. Indic.* **2022**, *142*, 109239. [CrossRef]

68. Turner, D.P.; Ritts, W.D.; Cohen, W.B.; Gower, S.T.; Zhao, M.S.; Running, S.W.; Wofsy, S.C.; Urbanski, S.; Dunn, A.L.; Munger, J.W. Scaling Gross Primary Production (GPP) over boreal and deciduous forest landscapes in support of MODIS GPP product validation. *Remote Sens. Environ.* **2003**, *88*, 256–270. [CrossRef]
69. Kim, J.H.; Hwang, T.; Yang, Y.; Schaaf, C.L.; Boose, E.; Munger, J.W. Warming-induced earlier greenup leads to reduced stream discharge in a temperate mixed forest catchment. *J. Geophys. Res. Biogeosci.* **2018**, *123*, 1960–1975. [CrossRef]
70. Jin, J.X.; Wang, Y.; Zhang, Z.; Magliulo, V.; Jiang, H.; Cheng, M. Phenology plays an important role in the regulation of terrestrial ecosystem water-use efficiency in the Northern Hemisphere. *Remote Sens.* **2017**, *9*, 664. [CrossRef]
71. Yu, Z.; Lu, C.Q.; Cao, P.Y.; Tian, H.Q.; Hessl, A.; Pederson, N. Earlier leaf-flushing suppressed ecosystem productivity by draining soil water in the Mongolian Plateau. *Agric. For. Meteorol.* **2018**, *250*, 1–8. [CrossRef]
72. Park, T.; Chen, C.; Macias-Fauria, M.; Tommervik, H.; Choi, S.; Winkler, A.; Bhatt, U.S.; Walker, D.A.; Piao, S.L.; Brovkin, V.; et al. Changes in timing of seasonal peak photosynthetic activity in northern ecosystems. *Glob. Chang. Biol.* **2019**, *25*, 2382–2395. [CrossRef] [PubMed]
73. Xu, C.Y.; Liu, H.Y.; Williams, A.P.; Yin, Y.; Wu, X.C. Trends toward an earlier peak of the growing season in Northern Hemisphere mid-latitudes. *Glob. Chang. Biol.* **2016**, *22*, 2852–2860. [CrossRef]
74. Ge, Z.X.; Huang, J.; Wang, X.F.; Tang, X.G.; Fan, L.; Zhao, Y.J.; Ma, M.G. Contrasting trends between peak photosynthesis timing and peak greenness timing across seven typical biomes in Northern Hemisphere mid-latitudes. *Agric. For. Meteorol.* **2022**, *323*, 12. [CrossRef]
75. Xu, X.J.; Du, H.Q.; Fan, W.L.; Hu, J.G.; Mao, F.J.; Dong, H. Long-term trend in vegetation gross primary production, phenology and their relationships inferred from the FLUXNET data. *J. Environ. Manag.* **2019**, *246*, 605–616. [CrossRef] [PubMed]
76. Wu, C.Y.; Peng, D.L.; Soudani, K.; Siebicke, L.; Gough, C.M.; Arain, M.A.; Bohrer, G.; Lafleur, P.M.; Peichl, M.; Gonsamo, A.; et al. Land surface phenology derived from normalized difference vegetation index (NDVI) at global FLUXNET sites. *Agric. For. Meteorol.* **2017**, *233*, 171–182. [CrossRef]
77. Wu, L.Z.; Ma, X.F.; Dou, X.; Zhu, J.T.; Zhao, C.Y. Impacts of climate change on vegetation phenology and net primary productivity in arid Central Asia. *Sci. Total Environ.* **2021**, *796*, 149055. [CrossRef]
78. Ma, X.L.; Zhu, X.L.; Xie, Q.Y.; Jin, J.X.; Zhou, Y.K.; Luo, Y.P.; Liu, Y.X.; Tian, J.Q.; Zhao, Y.H. Monitoring nature's calendar from space: Emerging topics in land surface phenology and associated opportunities for science applications. *Glob. Chang. Biol.* **2022**, *28*, 7186–7204. [CrossRef] [PubMed]
79. Nayak, R.K.; Patel, N.R.; Dadhwal, V.K. Estimation and analysis of terrestrial net primary productivity over India by remote-sensing-driven terrestrial biosphere model. *Environ. Monit. Assess.* **2010**, *170*, 195–213. [CrossRef] [PubMed]
80. He, H.L.; Liu, M.; Xiao, X.M.; Ren, X.L.; Zhang, L.; Sun, X.M.; Yang, Y.H.; Li, Y.N.; Zhao, L.; Shi, P.L.; et al. Large-scale estimation and uncertainty analysis of gross primary production in Tibetan alpine grasslands. *J. Geophys. Res. Biogeosci.* **2014**, *119*, 466–486. [CrossRef]
81. Tu, Z.Q.; Sun, Y.; Wu, C.Y.; Ding, Z.; Tang, X.G. Long-term dynamics of peak photosynthesis timing and environmental controls in the Tibetan Plateau monitored by satellite solar-induced chlorophyll fluorescence. *Int. J. Digit. Earth* **2024**, *17*, 2300311. [CrossRef]
82. Zhao, D.Y.; Hou, Y.Q.; Zhang, Z.Y.; Wu, Y.F.; Zhang, X.K.; Wu, L.S.; Zhu, X.L.; Zhang, Y.G. Temporal resolution of vegetation indices and solar-induced chlorophyll fluorescence data affects the accuracy of vegetation phenology estimation: A study using in-situ measurements. *Ecol. Indic.* **2022**, *136*, 108673. [CrossRef]
83. Wang, S.Y.; Wang, X.Y.; Chen, G.S.; Yang, Q.C.; Wang, B.; Ma, Y.X.; Shen, M. Complex responses of spring alpine vegetation phenology to snow cover dynamics over the Tibetan Plateau, China. *Sci. Total Environ.* **2017**, *593*, 449–461. [CrossRef]
84. Gao, B.; Li, J.; Wang, X.S. Impact of frozen soil changes on vegetation phenology in the source region of the Yellow River from 2003 to 2015. Theor. *Appl. Climatol.* **2020**, *141*, 1219–1234. [CrossRef]
85. Wang, Y.Y.; Ma, Y.M.; Li, H.X.; Yuan, L. Carbon and water fluxes and their coupling in an alpine meadow ecosystem on the northeastern Tibetan Plateau. *Theor. Appl. Climatol.* **2020**, *142*, 1–18. [CrossRef]
86. Zhang, Q.; Zhao, H.F.; Cheng, W.Y.; Cong, N.; Wang, X.H.; Liang, H.Q.; Li, X. Ncreased productivity of temperate vegetation in the preceding year drives early spring phenology in the subsequent year in northern China. *Sci. Total Environ.* **2023**, *903*, 166676. [CrossRef] [PubMed]